Research Article Vol. 36, No. 2 / February 2019 / Journal of the Optical Society of America B A139

Journal of the Optical Society of America B

OPTICAL PHYSICS

Supercontinuum radiation in fluorescence microscopy and biomedical imaging applications

CHETAN POUDEL AND CLEMENS F. KAMINSKI*

Department of Chemical Engineering and Biotechnology, University of Cambridge, Cambridge, UK
**Corresponding author: cfk23@cam.ac.uk*

Received 1 October 2018; revised 24 December 2018; accepted 28 December 2018; posted 3 January 2019 (Doc. ID 347224); published 25 January 2019

Compact, high brightness supercontinuum sources have already made a big impact in the fields of fluorescence microscopy and biomedical imaging techniques, such as optical coherence tomography and coherent anti-Stokes Raman scattering. In this review, we provide a brief overview on the generation and properties of supercontinuum radiation for imaging applications. We review specific uses of supercontinuum sources and their potential for bioimaging, but also their limitations and caveats. We conclude with a review of recent advances in UV supercontinuum generation, near-IR microscopy, exciting new potentials for the use of hollow-core PCFs, on-chip supercontinuum generation, and technologies to improve supercontinuum stability for certain applications.

https://doi.org/10.1364/JOSAB.36.00A139

1. INTRODUCTION

Fluorescence microscopy and biomedical imaging technologies have made enormous progress over the past two decades. An entirely new set of tools are available in the life sciences that permit targeted structural and functional information to be gained from biological systems. Exciting developments include superresolution methods [1–4] that go beyond the diffraction limit in optical imaging as well as methods that allow one to measure spectroscopic parameters, such as wavelength spectrum and fluorescence lifetime [5]. These techniques provide information not only on the location of sub-cellular structures but also on their function and environment. The field has been greatly boosted by technological developments in detectors and light sources, but also molecular labeling methods to permit specific staining of many different targets. The increasing sophistication of bioimaging experiments has placed an ever increasing demand on the enabling photonics technologies. One of the most groundbreaking developments over the past two decades in this context is the compact fiber-based supercontinuum (SC) source.

Exhaustive reviews on the topic of generating a SC and its properties already exist in the literature [6–11]. The freedom in design afforded by photonic crystal fibers (in tuning hole diameter, periodicity, core size, and material) has allowed scientists to use the interplay between dispersion, nonlinearity, optical losses, and polarization effects [9] to generate SC tailored for various applications. Additionally, a number of waveguiding mechanisms can be exploited—using total internal reflection in most solid-core fibers, the photonic bandgap effect in hollow-core (HC) fibers [12], and anti-resonance in some recently reported hollow fiber designs [13,14]. SC sources are often (erroneously) referred to as "white-light lasers." Temporally coherent and laser-like SC can be generated through short pulse pumping, but many useful SC sources for biological applications come from high-power, incoherent supercontinua, that are driven by longer pump pulses. Both types of SC radiation, coherent and incoherent, can provide high spatial coherence as they are usually generated by the fundamental mode of optical fibers. Average output powers of multiple watts are routinely achieved in commercial devices, making them suitable for many applications. SC sources have been employed in applications ranging from studies of fundamental processes in physics, biology, and chemistry [11] through absorption and excitation spectroscopy [15–18]; the generation of ultrashort femtosecond pulses to create optical clocks and frequency combs for precision frequency metrology (leading to a Nobel prize in 2005) [19]; optical communication; atmospheric science, and light detection and ranging [20]; biomedical imaging using optical coherence tomography (OCT) [21] and coherent anti-Stokes Raman scattering (CARS) [22]; and live cell imaging using various microscopy techniques [23]. In this short review, we present aspects of SC sources most relevant for the demands in microscopy (mostly fluorescence-based modalities) and for biomedical imaging applications. We begin with the properties of the SC that are critical in the context of imaging. We then provide an overview of methodologies used to select desired wavelengths, and

go on to review the wide variety of SC-enabled microscopies reported so far. These include widefield and laser scanning techniques, spectral imaging, lifetime imaging, two-photon absorption, superresolution, and OCT and CARS microscopies. We conclude with an outlook of current challenges in the field, and recent developments that may enable new applications in the future, including the use of gas-filled hollow-core fibers to generate tunable UV radiation with high pulse energies and peak powers.

2. PROPERTIES OF SUPERCONTINUUM RADIATION TAILORED FOR IMAGING

Ranka's [24] use of solid-core photonic crystal fiber (PCF) and a mode-locked Ti:sapphire laser, and Birks's report [25] on tapered optical fibers were the first demonstrations to herald the promise of efficient, cost-effective and routine generation of octave-spanning SC in the laboratory. The creation of endlessly single-mode PCFs supporting all generated wavelengths within one fundamental guided mode of the fiber [26] complemented these developments. Today, after over 40 years of theoretical and experimental research into SC generation, the spectral broadening mechanisms are understood and have been identified to be soliton dynamics, self-phase modulation, four-wave mixing, modulation instability, Raman self-frequency shift, and dispersive wave generation [11,27–29]. A SC can today be generated routinely using a range of fiber types, input pump sources, pulse energies, and input pulse durations ranging from femtoseconds (fs) to continuous-wave sources [7]. A SC generated by pumping PCFs can be broadly categorized according to the injected pulse durations, as (a) ultrafast fs pulses and (b) long pulses (picosecond–nanosecond [ps–ns] pulses or continuous wave), summarized in Table 1. This can be further sub-divided based on whether the SC generating medium is pumped in the normal dispersion (NDi) or anomalous dispersion (ADi) regimes. The dispersion regimes dictate SC generation mechanisms and propagation dynamics inside the nonlinear fibers. Therefore, choosing the right regime for desired output characteristics is critical, affecting not just the obtainable bandwidth and pulse durations but also properties of SC dynamics like coherence and shot-to-shot stability. In what follows, we discuss how these properties (spectral bandwidth, brightness, pulse energy, pulse duration, average power, coherence, and stability) can be controlled by selecting appropriate input pulses and dispersion regimes for specific applications, such as fluorescence microscopy.

SC generation over the last few decades was driven primarily by a push to increase spectral bandwidth and create octave-spanning wavelength spectra encompassing the full visible range and NIR. An efficient way of generating such broadband SC is by using fs pulses from Ti:sapphire (800 nm) lasers to pump tailored PCFs. These PCFs are fabricated specifically to place the input source wavelengths in the ADi regime, as in Ranka's experiment [24]. Owing to its enormous potential in optical imaging, this method was picked up already in 2004 by various biophotonics laboratories, reporting either the use of custom-built PCFs [30–32] or tapered silica fibers [33] in the ADi regime with hundreds of milliwatts of input power from ∼80 MHz Ti:sapphire lasers. The SC covered a broad wavelength spectrum from ∼400 nm to near-IR wavelengths of ∼1000–1500 nm because of efficient broadening via soliton dynamics. The spectral power densities were fairly low (less than 0.5 mW/nm) but usable for general fluorescence microscopy applications.

However, pumping in the ADi regime also leads to high instability arising from shot noise in the input laser pulses, which gets amplified stochastically by modulation instabilities [7]. This leads to temporally incoherent SC light with uneven spectra and large differences in spectral density profiles from shot-to-shot (see Fig. 1). SC instability does not necessarily pose a problem in general fluorescence microscopy applications since the time scale of experiments is much longer than the instantaneous fluctuations, causing them to be averaged over. Temporally incoherent light is, in fact, often favored for imaging because coherent waves can introduce unwanted speckle patterns in the image. On the other hand, applications such as CARS need a high degree of coherence, for which fs pumping of all-NDi fibers is more suitable since modulation instability and soliton-related effects do not occur in this case. This generates a stable, flat, and coherent SC with much better signal-to-noise [34,35], albeit with smaller spectral widths at comparable peak power [36].

A big limitation in using fs pumps is the maximum obtainable SC power. The peak intensity damage threshold in microstructured fibers usually limits the maximal output spectral power density to ∼0.5 mW/nm. For applications requiring higher power densities, using ps–ns input pulses, this increases to several milliwatts per nanometer in the visible range [37]. Of course, when longer pulses are used as input pump sources, the instability problem is greater (both in the NDi and ADi regimes): larger fluctuations are seen, and the coherence of the SC is compromised. Despite the stability issue, the rapid

Table 1. General Characteristics of Different SC Generated by Altering Pump Sources

Pulse Duration	Femtosecond Pulses	Pico-Nanosecond Pulses and Continuous Waves
Spectral width	Broad spectrum (visible-NIR)	Broad spectrum when using pulsed input, some covering 400–2400 nm; mostly only IR spectrum for CW sources
Coherence and stability	Coherent and stable (NDi regime); incoherent, unstable (ADi regime)	Usually incoherent, unstable but can be coherent with ps sources (NDi regime); large fluctuations, incoherent for CW
Spectral power density	Low, around 0.5 mW/nm	Moderate values for ps–ns pulses, around few mW/nm; high power for CW: 10 s of mW/nm
Pump peak power	fs input: few kW	ps–ns input: usually 100 s of W; CW input: few W
Convenience	Usually very expensive, complex, and difficult to maintain	Cost-effective and low maintenance. Widespread applications for pulsed output.

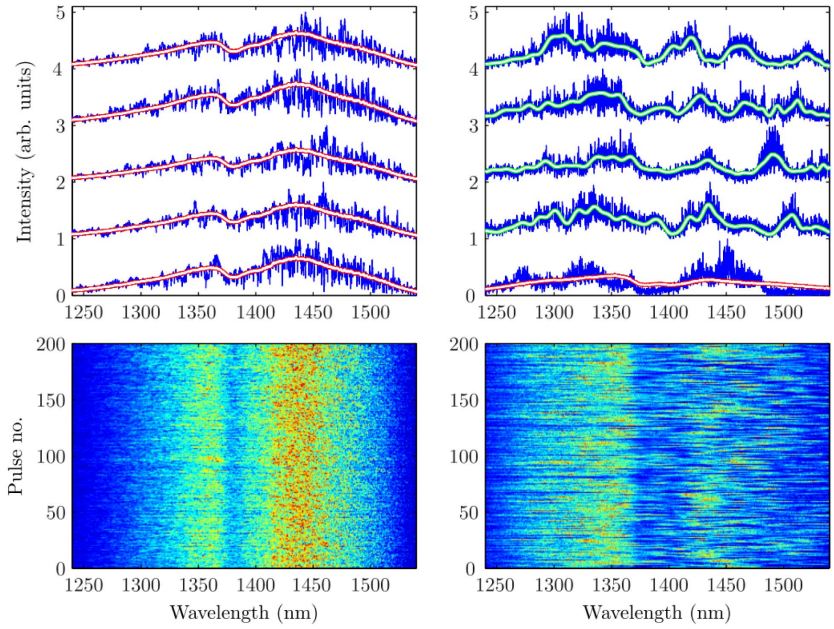

Fig. 1. Comparison of shot-to-shot differences in SC spectra obtained with femtosecond pumping in the normal dispersion (NDi—left panels) and anomalous dispersion regimes (ADi—right panels). The red/white lines (top left) represent a long-term average (10,000 shots) of the all-NDi spectrum, where each individual shot trace (blue) mimics the shape of the average long-term spectrum. This stability in the NDi regime can also be observed in the 200 consecutive single-shot spectra (bottom left). The green/white lines (top right) are low-pass filtered versions of individual shot-to-shot spectra, all of which show significant deviations from their long-term average (red/white line in the bottom) in the ADi regime SC. Consecutive single-shot spectra also show large differences (bottom right) in the ADi regime. Clearly, the dynamics of SC in the NDi regime are in stark contrast with dynamics in the ADi regime. Adapted from [34].

development of fiber laser sources over the last ten years has provided cost-effective, reliable means of providing ps–ns input pulses for SC generation with low maintenance and smaller fingerprint than fs sources. Therefore, for microscopy and bioimaging applications, generation of a SC has mostly switched over to using these ps–ns fiber laser pump sources. The technology has also been commercialized by a few companies making SC widely accessible and usable by general biology laboratories through a variety of compact turn-key sources [22]. As an example of commercial technology, a widely established incoherent SC source is based on coupling ps pulses from a mode-locked (typically 40 MHz) ytterbium fiber laser into an engineered PCF with a zero dispersion wavelength (ZDW) around 1050 nm. This yields average SC output powers reaching ~20 W with 6 ps pulse widths, few 100 nanojoules maximum pulse energy, and single-mode operation in the 400–2400 nm range [38]. Research groups working on higher average output from ps sources have reached powers up to 39 W, with 31.7 mW/nm spectral power density and good uniformity across the full visible spectral range [39].

A SC has also been generated using continuous-wave sources like fiber lasers using simple, cost-effective setups yielding broad spectral profiles. Massive output power densities (10 s of mW/nm) can be generated from 5 to 50 W pump sources and used in applications where high average brightness is more important than short-pulse characteristics. However, a SC generated from CW input undergoes significant intensity fluctuations and has negligible temporal coherence due to modulation instability [7]. The spectral coverage usually lies in the NIR with bandwidth not large enough to extend into the visible range. This is one of the biggest limitations of CW input for SC generation as obtaining output in the visible spectrum is of prime importance in applications like fluorescence microscopy. Some attempts have been made to increase bandwidth and simultaneously push it toward the visible range going down to 600 nm [40], but this required industrial class fiber lasers to provide enormous pump powers of 400 W, which is impractical for routine use. Another concept for extending to shorter wavelengths in CW SC was demonstrated through fiber tapering, causing dispersive waves to be further blueshifted. A wavelength extending to 650 nm can thus be reached even with moderate pump powers of around 35 W [41]. Finally, through Ge-doping and fiber tapering, the first pure CW white-light SC was generated in 2012 with a spectrum spanning from 470 nm to more than 1750 nm at 9.3 W power [42].

3. WAVELENGTH SELECTION SCHEMES

Perhaps the most useful property of a SC source in fluorescence microscopy lies in its massively broadband wavelength spectrum. Traditionally, fluorescence studies of cellular processes have used mercury and xenon arc lamps for broadband illumination. These suffer from low illumination efficiency and low spatial coherence, and therefore cannot be used to improve resolution in scanning-microscopy applications. Diodes and monochromatic lasers provide bright illumination but without the necessary broad bandwidth. The handful of monochromatic lasers that are commonly available pose an unnecessary

restriction on the vast available toolbox of excitable fluorophores, rendering only a few fluorophores usable whose excitation wavelengths match the fixed laser wavelengths. Even then, the most efficient excitation wavelength can lie between available laser wavelengths [23].

The increasing complexity of bioimaging experiments and rising demand to simultaneously image in multiple colors necessitate flexible use of excitation wavelengths across the entire visible range to avoid cross talk. Previously, dye laser systems with tunable wavelengths have been used [43] to excite multiple fluorophores, but the gain curves of these dyes limit the tuning range to 50–100 nm and do not cover a significant portion of the visible spectrum. Tunable Ti:sapphire lasers provide another alternative to access the full visible spectrum but they can only achieve this through processes like multi-photon absorption, harmonic generation, and using optical parametric oscillators (OPOs), making the process expensive and difficult to operate, and requiring specialist maintenance. SC sources overcome most of these spectral restrictions with a large bandwidth spanning the visible and NIR without any gaps, and thus lifting the restrictions of matching fluorophores to available laser lines. The full SC spectrum is rarely used simultaneously for imaging. Most fluorescence applications pick out desired excitation wavelength bands from the output. While this means that most of the power is discarded, the average power of the spectrally selected output (~1 mW/nm from commercial sources) is still sufficient for most imaging applications [31]. In conjunction with versatile wavelength selection schemes, a SC source can simultaneously excite a number of fluorophores, each at their optimal absorption wavelengths. This provides high specificity with minimal cross-excitation and permits studies of various structures and phenomena at the same time.

Good wavelength selection schemes should provide full flexibility in selecting wavelengths and bandwidth over a large spectrum at high speed with potentials for multiplexed imaging. Many such technologies have been proposed but the most noteworthy ones (see Fig. 2) include bandpass filter wheels, prism-based spectrometers [31], axial monochromators [44], motorized linear variable tunable filters (LVTFs) [45], and acousto-optic tunable filters and beam splitters (AOTFs and AOBSs) [46,47]. In Table 2, we summarize and compare the characteristics of these technologies.

Using a filter wheel with 6–12 bandpass filters can accommodate a wide range of wavelengths. The high-precision multilayer coatings on these filters provide excellent out-of-band suppression (usually over OD 5) and high edge steepness. However, changing wavelengths requires physical movement of the filter wheel in the beam path over 50–200 ms time scale (when motorized), precluding the possibility of simultaneous multi-wavelength selective excitation. Dual, triple, or quad band filters are now available for performing simultaneous excitation but these are not tunable for arbitrary selection. A different tunable implementation uses prisms to spatially disperse the beam, part of which goes through a translatable aperture to select a central wavelength and bandwidth [31], but this leads to large power losses and does not allow simultaneous excitation

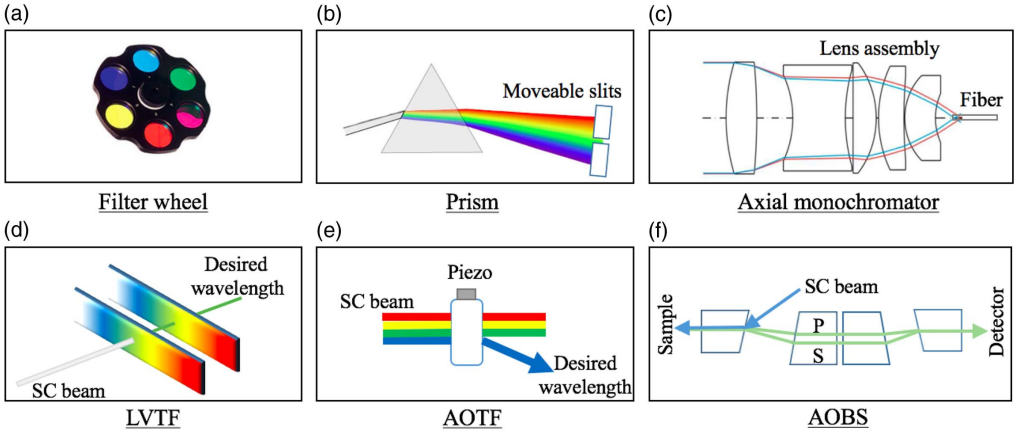

Fig. 2. Different schemes to select desired excitation bands from SC sources: (a) filter wheel, (b) prism [31], (c) axial monochromator [44], (d) LVTF [45], (e) AOTF [46], and (f) AOBS [47]. Their individual characteristics are summarized in Table 2.

Table 2. Wavelength Selection Schemes with Their Pros (+) and Cons (–)

Characteristics	Filter Wheel	Prism	Axial Monochromator	LVTF	AOTF	AOBS
High transmission	+	–	+	+	–	+
Tuning speed	–	–	–	–	+	+
Wide wavelength range	+	+	+	+	+	+
Tunable bandwidth	–	+	–	+	–	–
Simultaneous multi-color	–	–	–	–	+	+
Out-of-band suppression	+	+	+	–	–	–
Steep spectral edge	+	–	–	–	–	–
Polarization insensitive	+	–	–	+	–	+

of multiple wavelength bands. Another excitation technique uses an on-axis monochromator based on a custom-designed lens to intentionally maximize the beam's longitudinal chromatic aberration while keeping other aberrations low [44]. This wavelength-dependent longitudinal dispersion of foci along the optical axis allows coupling the desired part of the focused beam into a finite aperture fiber and discarding all other out-of-focus wavelengths.

To continuously tune the central wavelength along with bandwidth, one can use LVTFs whose cutoff wavelengths vary linearly along their length. A useful configuration involves the SC beam going through two LVTFs (one as short-pass, one as long-pass) translated independently to make a variable bandwidth filter [45]. Circular LVTFs use the same concept but work by rotating the filters. LVTFs work well for tuning excitation when the optical beam width is small in cross section as finite beam widths deteriorate the edge steepness. The need for mechanical translation slows their tuning speed (~ hundreds of milliseconds) and they cannot be used for simultaneous wavelength selection.

In contrast to previous technologies, AOTFs provide very fast, programmable wavelength tuning (microseconds) with simultaneous output possible for up to eight different wavelengths over a large spectral range (hundreds of nanometers) with no moving parts, demonstrated [48] for spectrally resolved imaging. Acousto-optic technologies effectively produce a phase grating to diffract a specific part of the incident light with very narrow passband (~1 nm) under phase-matching conditions of optical and acoustic waves. However, AOTFs do suffer from low out-of-band suppression, low transmission due to polarization selectivity, and sometimes from wavelength sidebands that introduce a wavelength-dependent angular spread in their output [48], which degrades image quality. Additional compensation optics like prism elements can correct for polarization selectivity to restore high transmission and remove angular spread, and have been commercialized as AOBS [33,47], making them a single versatile instrument handling both excitation and emission selection efficiently.

No single wavelength filtering scheme fulfills the needs of all imaging experiments, although acousto-optic technologies provide more versatility than others. It is important to evaluate and choose wisely between them by considering the criteria (e.g., speed, tunability, out-of-band suppression to minimize cross talk, and simultaneous multi-color) most relevant for the experiment. Once spectral selection is performed appropriately, the output light can be coupled to a microscope directly for widefield imaging, or via a beam scanning unit for point-scanning, or modified in other ways (e.g., beam shaping, pulse compression) for desired applications.

4. MICROSCOPY MODALITIES USING SUPERCONTINUUM RADIATION

SC sources have revolutionized microscopy for biological and medical imaging applications, offering significant advantages over monochromatic lasers in spectral flexibility and over traditional lamp sources in terms of fast pulsed nature, high brightness, spatial coherence, deep tissue penetration and contrast [49]. In what follows, we discuss how SC properties are exploited in different microscopy applications. We review the use of SC spectral flexibility, particularly in hyperspectral imaging; SC spatial coherence for point-scanning microscopies; the fast pulsed nature of a SC for spectroscopy and fluorescence lifetime imaging (FLIM); high peak power applications in multi-photon excitation and second-harmonic generation (SHG); simplification of superresolution microscopy instrumentation using SC sources; and finally, the bright, coherent light applications of a SC for OCT and CARS microscopies.

A. Widefield and Confocal Scanning Techniques, and Wavelength-Resolved Imaging

SC sources provide a wider spectrum of wavelengths and much greater brightness than thermal sources or LEDs for widefield fluorescence microscopy techniques. In particular, an incoherent SC is best for widefield imaging since it provides flat-field illumination without generation of speckle artifacts or aberrations. These artifacts are seen with traditional coherent laser sources due to interference between light waves and they degrade image quality [50,51]. Incoherent SC with large spectral bandwidth and excellent beam profiles are marketed commercially, permitting easy integration into traditional setups for widefield microscopy. The SC output can additionally be launched into a multi-mode fiber to impose a strong spatial incoherence and uniform illumination field. SC sources have found a greater market in confocal laser scanning fluorescence microscopy, which was the first bioimaging application to adopt SC radiation [30,31]. This is because fiber-generated SC radiation can easily be focused onto a diffraction-limited spot and point-scanned through the sample. It is conceivable that high-power commercial SC sources will replace monochromatic lasers in all future confocal microscopes, simplifying the setup, reducing costs, and enhancing versatility [37]. It is important to consider the effect of longitudinal chromatic aberration and chromatic variations in beam divergence potentially affecting the spatial resolution. A study quantifying and comparing 3D point spread functions (PSFs) in the blue and red spectral regions in a confocal setup utilizing a commercially available SC source found that the displacement of the focal spot along the z-axis was comparable in extent to the full width at half-maximum of the PSF [48]. Therefore, chromatic aberrations caused by using a SC source do not pose a significant limitation for performing high-resolution confocal imaging in multi-color throughout the visible spectrum. In other techniques, such as volumetric confocal reflectance microscopy [52], this chromatic aberration feature has been maximized using aspheric lenses because it permits one to encode depth information spectrally and to be read out by a spectrum analyzer or spectrometer. This way, multiple depths in a biological specimen can be probed simultaneously and rapidly, with one group demonstrating a 157 μm axial range with micrometer resolution captured in a single shot from epithelial tissue [53]. This technique eliminates the need for mechanical axial scanning, making it useful even for endoscopic imaging systems.

Combining the flexible excitation from a SC with appropriately multiplexed emission detectors enables the method of hyperspectral imaging (wavelength-resolved imaging over a continuous spectral range; see Fig. 3). Hyperspectral imaging allows capturing and completely characterizing the entire

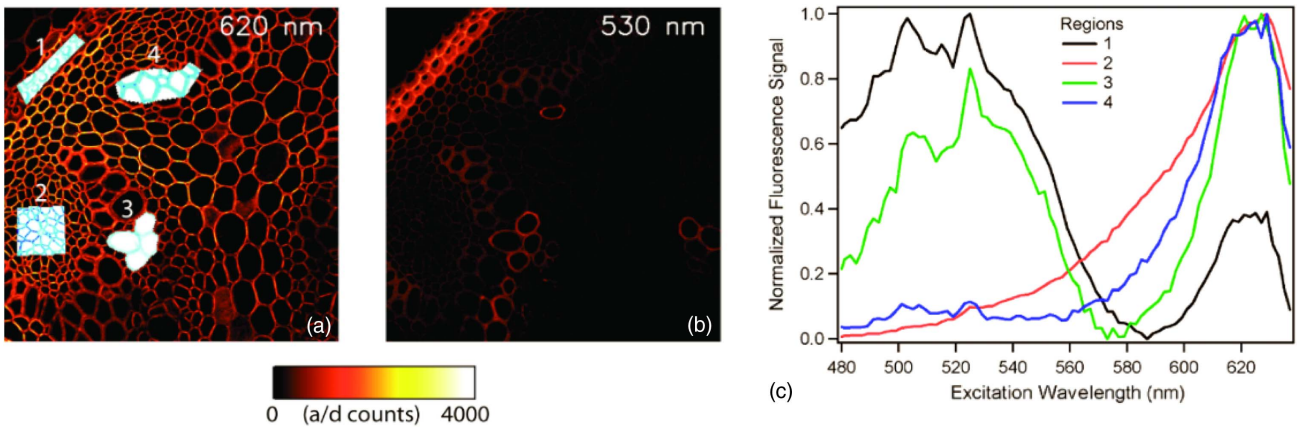

Fig. 3. Hyperspectral imaging reveals that different regions of *Convallaria majalis* have different emission properties at (a) 620 nm and (b) 530 nm excitations. (c) Excitation-emission plots for four regions in (a). Adapted from [54].

excitation and emission profile of known and unknown fluorophores and biological samples at all available wavelengths for each pixel of the image [23,54,55,56]. This information can be used in post-acquisition spectral unmixing methods to reliably discriminate fluorophores with overlapping spectra in biological studies [57,58]. The same technique can be used to remove unwanted autofluorescence in the emission channel that might be affecting the data. In other cases, tissue autofluorescence may contain useful information. Tissues undergoing disease progression can show structural and metabolic changes affecting their absorption, scattering, and fluorescence characteristics [59], and these subtle changes can be picked up by SC-based hyperspectral imaging techniques. This has been particularly successful in label-free imaging of biological specimens. Probing for more spectral information using a SC at extended wavelengths and increased acquisition rates will greatly enhance noninvasive disease diagnostics [60].

B. Fluorescence Lifetime Microscopy and Multi-Parameter Imaging

The inherent pulsed nature of most SC sources is useful for time-resolved fluorescence spectroscopy. This technique can measure the excitation and emission spectra of fluorophores, along with the average lifetime of their fluorescence decay with a high-temporal (sub-ns) resolution. The fluorescence decay lifetime of fluorophores is exquisitely sensitive to their microenvironment and can provide quantitative information about the pH, local viscosity, temperature, ion concentration, protein aggregation, protein binding, and kinetics of chemical reactions around the fluorophores [5,61]. SC sources provide the high-frequency (~MHz) pulsed excitation required for lifetime measurements and now some commercial sources also offer easy tuning of this repetition rate (80, 40, 20, 10, 5, etc., in megahertz) for capturing shorter or longer lifetimes. The short pulse width (few ps) of the SC output helps reduce errors in temporal measurements. Selecting narrow bands from the SC spectrum also allows specificity in exciting fluorophores with distinct spectra and lifetimes at their optimal absorption wavelengths. SC sources can replace fast-pulsed flash lamps in spectrofluorometers [62], providing higher brightness to improve signal-to-noise ratios for sensitive measurements. Merging the capabilities of spectrofluorometry with spatial imaging leads to a powerful quantitative imaging technique called FLIM. Several implementations of FLIM using SC radiation are in use, including widefield- and spinning-disk-based systems (time-gated FLIM [63,64] and frequency domain FLIM [65,66]), and the more popular point-scanning-based time-correlated single-photon counting (TCSPC) FLIM systems [31]. All these FLIM implementations can provide the spatial distribution of fluorophores, and their individual percentage contribution to fluorescence in each image pixel.

Like hyperspectral imaging, unmixing multiple fluorophores in an image can be done using fluorescence lifetime as a parameter, even with minimal *a priori* information [67]. FLIM can also be applied to reveal the intrinsic lifetime contrast (see Fig. 4) to investigate health states of tissues. The autofluorescence lifetime characteristics can be studied by simply exciting endogenous fluorophores without labels [5,61] at desired wavelengths using a SC source. SC sources have opened up a more practical way to study Forster resonance energy transfer (FRET) using FLIM to observe complex protein interactions, protein structures, and molecular conformations at high speeds in live cells [68]. By minimizing cross-excitation of acceptors, SC sources enable multi-channel FLIM-FRET [69] from the same laser source. Some advanced FLIM setups using a SC can capture multiparametric and hyperspectral 6D [56] and 7D [55] data with not just the spatial profile and absorption-emission spectra but also simultaneously the fluorescence lifetime and polarization anisotropy profiles (x, y, z, λ_{ex}, λ_{em}, τ, r) for each pixel. This presents opportunities to improve studies of multiplexed signaling pathways, tissue properties, and functional aspects at the molecular scale.

While the temporal instability of incoherent SC sources may be an issue in certain applications, fluorescence lifetime measurements are mostly unaffected by the shot-to-shot variations because this noise is small compared to the photon-shot noise in imaging systems. In the most widely used TCSPC implementation, only a small fraction of excitation pulses generate a detectable photon to avoid photon pileup effects. On the time scales of TCSPC FLIM image acquisition (seconds to minutes), the average power of the SC is fairly stable [31]. However, other techniques, such as fluorescence correlation spectroscopy

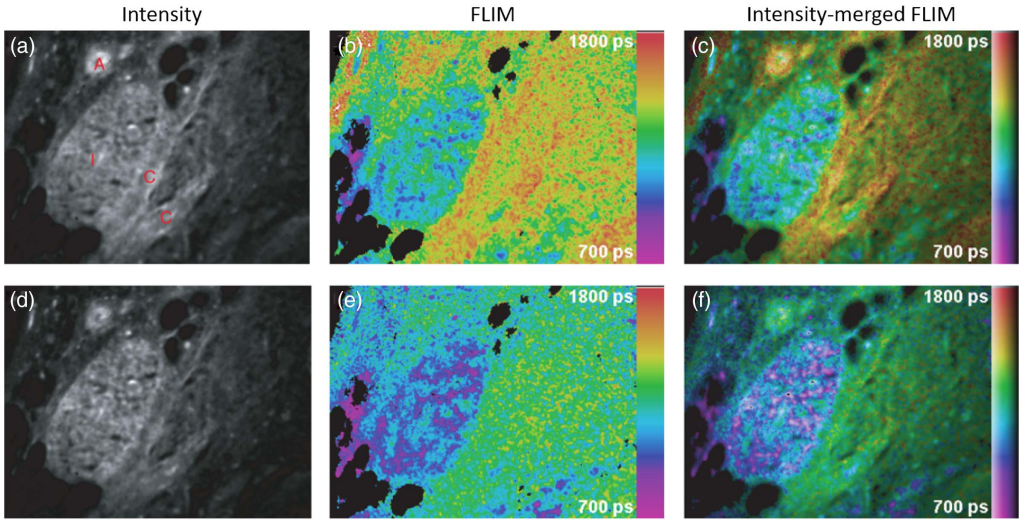

Fig. 4. Intensity and intensity-merged FLIM images of autofluorescence from a section of unstained human pancreas showing clear lifetime differences between tissue types: A, artery; I, islets of Langerhans; and C, collagen connective tissue. (a)–(c) $\lambda_{ex} = 440$–450 nm, $\lambda_{em} > 470$ nm. (d)–(f) $\lambda_{ex} = 520$–530 nm, $\lambda_{em} > 570$ nm. Adapted from [31].

(FCS), require much more stable lasers and cannot make use of the SC radiation used for most imaging applications, produced by pumping PCFs in the ADi regime. FCS as a technique relies on detecting fluctuations in fluorescence intensity from a small sample volume and therefore, any fluctuations stemming from varying laser illumination will introduce errors in the acquired FCS curve, negatively affecting the experimental outcome [70]. Despite this caveat of instability, other SC features like spectral tunability, simplicity, and cost-effectiveness have made the fiber-laser-pumped SC a more attractive option than multiple laser lines or mode-locked Ti:sapphire lasers in many FLIM and multi-parametric imaging applications.

C. Superresolution Microscopy: Stimulated Emission Depletion

The ability to arbitrarily choose and rapidly change excitation wavelengths using a SC source greatly enhances the number of usable photoactivated dyes and fluorophores [71]. These fluorophores can be turned on and off with different wavelengths and form the basis of many superresolution techniques, such as photoactivated localization microscopy (PALM), stochastic optical reconstruction microscopy (STORM), and stimulated emission depletion (STED), among others.

The high illumination densities (~5 kW/cm^2) necessary for PALM and STORM [3,4] require very high laser powers (~50–100 mW) at specific wavelengths, which is not easily attained using SC sources. However, STED instrumentation greatly benefits from the simplicity, easy maintenance, and affordable cost of a SC source. STED uses one laser pulse focused onto a diffraction-limited spot for fluorophore excitation. A few ps later, the excitation pulse is followed by a donut-shaped red-shifted laser pulse to de-excite fluorophores through stimulated emission (see Fig. 5). Only a few fluorophores confined in a sub-diffraction-sized donut center are allowed to fluoresce, improving the imaging resolution beyond the diffraction limit [1] and reaching resolution below 50 nm. A pulsed tunable SC source used for STED can include wavelength ranges not covered by common pulsed laser sources [72], opening the possibility of using an increased range of fluorophores [73]. The SC also provides both the excitation and depletion wavelength

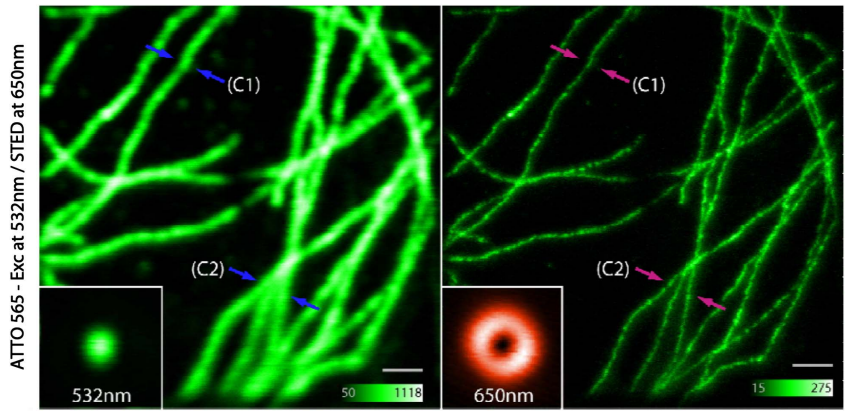

Fig. 5. STED of immunolabeled tubulin fibers with 532 nm excitation and 650 nm depletion donut beam obtained from a single SC source. Comparing between confocal image (left) and STED (right) shows the resolution enhancement with STED. Adapted from [72].

bands from the same source, eliminating the second laser entirely. Easy and stable temporal alignment can be achieved without the need for synchronization of multiple excitation and depletion sources. SC sources also readily provide ps pulse width output, which is most efficient for STED, obviating the need for pulse-stretching of fs range pulses given by Ti:sapphire lasers. Thus, SC sources allow making major simplifications to the very complicated instrumentation, which is one of the primary drawbacks of STED microscopy. In an example from a few years ago, simultaneous two-color STED was demonstrated for the co-localization of two different proteins at super-resolution (35 nm lateral, 90 nm axial resolution) in three dimensions with a single commercial SC source (SC-450-PP-HE) instead of four very-expensive pulsed laser sources that would normally be required [74]. This SC source provided pulse energies (20 nJ for 20 nm bandwidth at 1 MHz) comparable to that of lasers commonly used in STED but the acquisition speed was limited by the low repetition rate. Improving resolution at greater speeds with STED depends on very efficient depletion with high pulse powers and therefore will benefit from improved SC sources providing greater pulse powers even at higher repetition rates. However, the main drawback in using a SC for STED is the large fluctuation in the pulse energy, which can vary from 10% to 80% and can induce large optical noise and hinder certain applications [7]. Balanced detection schemes might be able to reduce the noise down to shot-noise levels in these cases.

D. Two-Photon Excitation Microscopy and Second-Harmonic Generation

Achieving greater peak powers in custom-built SC sources has permitted two-photon excitation (TPE) microscopy with these sources. TPE is caused via the absorption of two photons, each around twice the wavelength of a single photon excitation event [75,76]. This allows probing into deeper tissue by using red-shifted wavelengths to increase penetration depth and minimize scattering and photodamage. This technique has been valuable in neuroscience and in medical studies involving imaging *in vivo* or in thick tissues. However, TPE is a nonlinear process requiring high photon fluxes in a small confined focal volume (using large peak powers at the sample and typically at least 0.01–0.1 nJ energies for laser scanning) in a very short timeframe. It has traditionally only been possible using mode-locked femtosecond lasers that compress the high laser power into ultrashort fs pulse packets. By giving out one intense pulse every 10–25 ns, these lasers manage to excite two-photon processes while keeping average power into the sample relatively low to avoid photobleaching and phototoxicity. When femtosecond input pulses are pumped through microstructured fibers, in addition to wavelength broadening, they also exhibit dramatic temporal broadening to yield output pulse durations of a few ps, but the pulse energies and peak intensities can still be large enough for TPE.

Two-photon excitation using a SC was achieved more than a decade ago by using the near-IR part of the spectrum (17 W peak power and 1.7 GW/cm^2 at the sample, sufficient for TPE even with pulse lengths of 1–5 ns) [33]. Others used the visible range of the SC (500–600 nm) [32] and used pulse compression techniques to increase peak intensities [77]. Simultaneous three-color TPE was also demonstrated using fs pulse SC output and 8 mW power at the sample [78]. However, in all these cases, generating a SC with the appropriate characteristics for TPE required pumping PCFs with the fs Ti:sapphire lasers, making them impractical in most general biology laboratories. The challenge, then, is for longer-pulse SC sources to generate the power densities required for TPE. Lefort *et al.* [79] demonstrated that both TPE and SHG are possible from a compact broadband SC source with ns pulses and sufficient peak power. Image quality (see Fig. 6) using the SC source (1 ns pulses with 370 nJ energy, 370 W peak power, 92 mW average power) was comparable to that obtained with a Ti:sapphire (150 fs pulses with 70 pJ energy, 460 W peak power, 5.5 mW average power). Over the years, as novel fibers and ns pump source technologies become mature, TPE should be widely accessible using

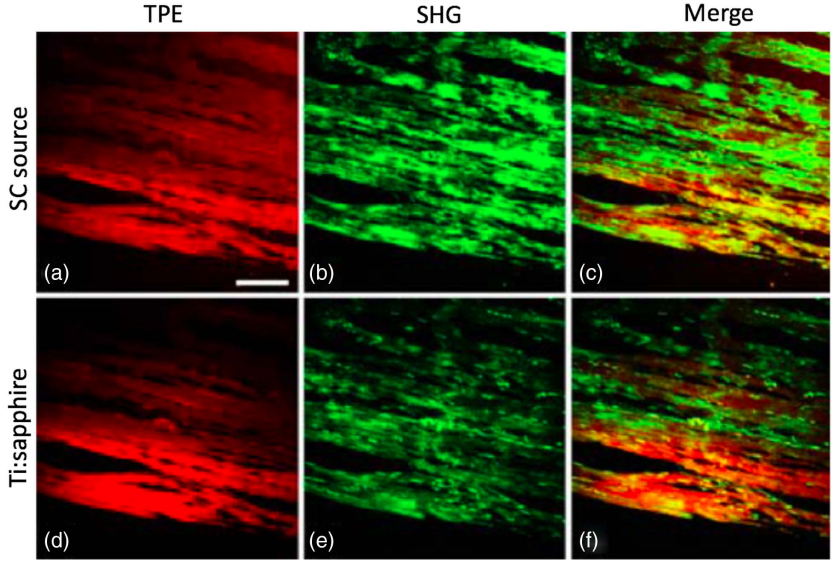

Fig. 6. Two-photon excitation of fluorescence, second-harmonic generation, and merge images of mouse muscle, comparing the performance of a nanosecond SC excitation (a)–(c) against femtosecond Ti:sapphire excitation (d)–(f). Adapted from [79].

compact and stable turn-key SC sources that provide large spectral densities with higher peak powers and intensities.

E. Optical Coherence Tomography

Optical coherence tomography is a noninvasive optical analog of ultrasound techniques, enabling depth-resolved imaging of biological tissues (see Fig. 7) at micrometer-scale resolution by using interferometric detection of photon time of flight [37]. Nowadays, OCT is routinely used in the diagnosis of retinal diseases [81]. OCT ideally requires a stable and noiseless, spatially coherent source with low temporal coherence, single transverse mode, and high brightness (power of few milliwatts per nanometer). The axial resolution of fine microstructures in OCT scales as $\lambda^2/\Delta\lambda$, depending inversely on the bandwidth [82], and thus benefits greatly from a source with long-range NIR bandwidth. These requirements are difficult to fulfill and in the past, superluminescent diodes and thermal sources were used for their bandwidth to provide 10–15 μm axial resolution. However, the low brightness of these sources limits their use in clinical OCT, as higher brightness is necessary to counter signal attenuation in strongly scattering biological tissue and to reduce the integration time in real-time imaging of *in vivo* tissues [60].

SC sources fulfill most of the necessary criteria listed above and have been shown to improve resolution by an order of magnitude, while providing higher brightness and faster acquisition in state-of-the-art high-resolution OCT measurements. While resolution can also be improved by using highly specialized broad-bandwidth, ultrashort-pulsed, mode-locked Ti:sapphire lasers, the expense and expertise these require are limiting. OCT researchers began to show an interest in SC generation after 2001 when ultrahigh-resolution OCT (resolution of 2.5 μm) was demonstrated from a SC source built using microstructured fibers pumped with a mode-locked Ti:sapphire laser [21]. Nowadays, SC radiation optimized for OCT is available even from compact commercial sources using fiber and microchip lasers, which can inexpensively provide a broader spectral coverage than Ti:sapphire lasers. These new SC sources cover several interesting spectral bands, such as the visible range for maximum biological chromophore absorption and submicrometer ultrahigh-resolution OCT, the 1.05 μm range for ophthalmic OCT with enhanced penetration depth and reduced scattering, and the 1.3–1.7 μm range for *in vivo* noninvasive biopsies [83]. Additionally, the broad bandwidth can be exploited to perform spectroscopic OCT. However, an ultrabroad SC generated from an interplay of various nonlinear effects in the ADi regime still suffers from instability (shot-to-shot variations) and uneven (non-Gaussian) spectral profile, leading to multiple image echoes hiding weak object structures and reducing the resolution and sensitivity. Pulse shaping implementations have been used to create Gaussian spectra but this comes with large losses in output power. A noteworthy attempt to reduce noise while simultaneously shaping the pulse without much loss has used appropriate tapering of PCFs to manipulate fiber dispersion to be in the NDi regime for all wavelengths, eliminating modulation instability and soliton effects [84]. Going forward, improving the stability of a SC generated from longer pump pulses is the key to compact, cost-effective yet high-performance OCT.

F. Coherent Anti-Stokes Raman Scattering Microscopy

Other useful biological imaging applications of SC sources are CARS microscopy and CARS microspectroscopy—techniques allowing visualization of chemical composition and structures of samples, based on their characteristic intrinsic vibrational contrast. CARS is label-free and has a nondeteriorating signal, unlike fluorescence where photobleaching eventually causes a large reduction in the SNR. CARS microscopy requires two beams (a pump pulse and a synchronous broadband Stokes pulse) and produces a signal when their difference matches the Raman resonance frequency of the sample [85]. These synchronous beams are difficult to produce without using two synchronized lasers or complex setups involving an optical parametric amplifier (OPA) and optical parametric oscillators (OPOs), or four-wave-mixing-based sources, which are the current state-of-the-art methodologies. However, these beams are also readily produced through SC generation [86] using fs lasers pumping PCFs tailored to produce appropriate wavelengths. Temporally coherent SC radiation has so far only provided low peak powers and low spectral power density. For a reasonably high-resolution CARS image, this poses a severe limitation of long acquisition times [87].

However, other techniques, such as multiplex CARS, do not require high temporal coherence. Incoherent and

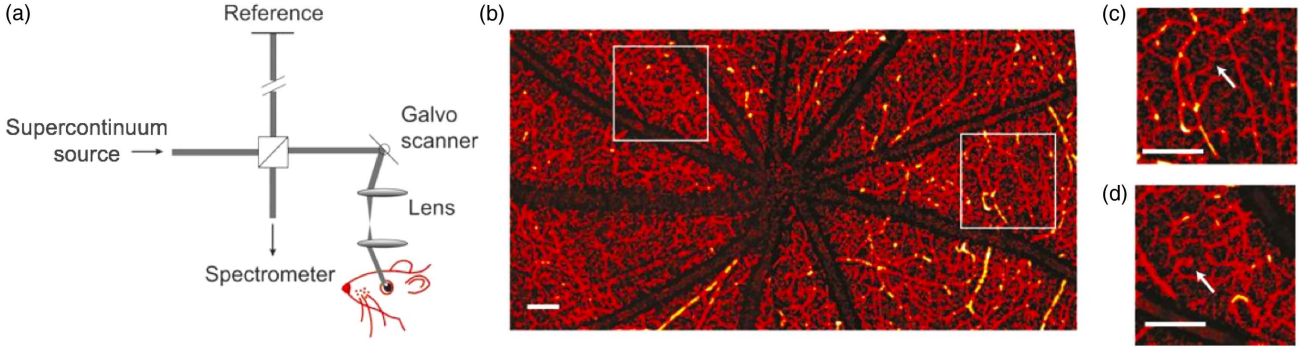

Fig. 7. (a) Schematic of an OCT setup using visible light (520–630 nm) from a commercial SC source for *in vivo* retinal imaging to measure oxygen metabolism. (b) Widefield view of retinal micro-vasculature imaged using this setup. (c)–(d) Magnified view of highlighted areas in (b), with arrows showing the smallest capillary vessels. Scale bar: 200 μm. Adapted from [80].

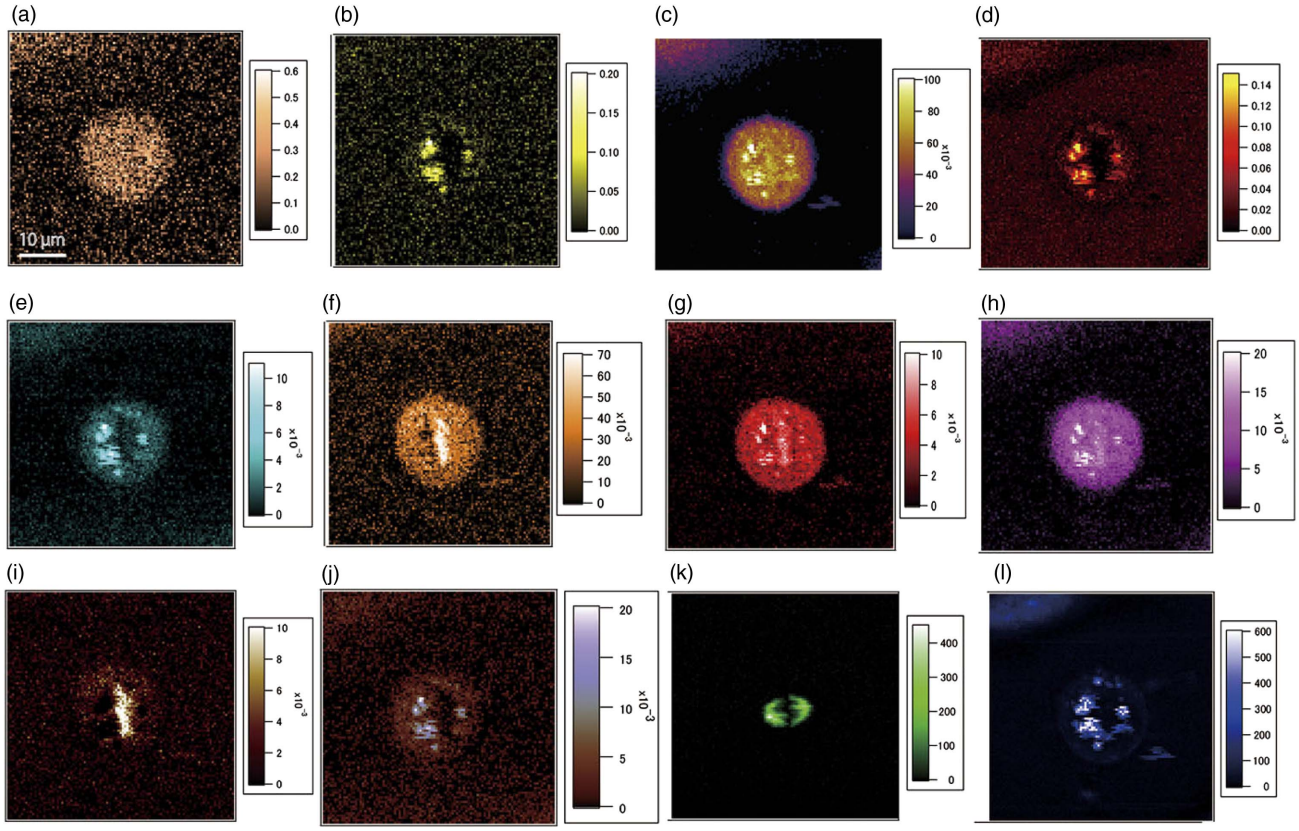

Fig. 8. CARS, second-, and third-harmonic generation images of a HeLa cell in the mitotic phase. Chromosomes appear in a line in the center of the cell in the DNA/RNA images and spindle fibers are seen in the SHG images. CARS images at (a)–(j) 3063 (proteins), 3010 (lipids), 2930 (proteins/lipids), 2851 (lipids), 1738 (lipids), 1574 (DNAs/RNAs), 1098 (DNAs/RNAs), 1004 (proteins), 791 (DNAs/RNAs), and 719 cm^{-1}, and the (k) SHG and (l) THG images. Adapted from [90].

ultrabroadband SC generated in the ADi regime using longer pulses and greater peak powers is ideally suited for multiplex CARS, especially when multiple signals can be generated and detected hyperspectrally [88]. Multiplex CARS microscopy with sub-micrometer resolution has been demonstrated [89] from a broadband SC (>2000 cm^{-1}). This has been combined with TPE of fluorescence [85], SHG and third-harmonic generation (THG) signals [90], to study proteins and lipids in cells (see Fig. 8). This multiplexed nonlinear approach permits different types of contrast to be achieved simultaneously to study dynamics of living cellular structures. Even compact, turn-key solutions are commercially available now that use a IR SC [22] for such multi-modal imaging.

5. CHALLENGES AND RECENT ADVANCEMENTS

It is clear from the various applications mentioned above that the useful features of compact SC sources, such as spectral flexibility, high spectral power density, fast pulses, low cost, low maintenance, and small footprint, have had a significant impact in biological and clinical imaging research. Despite their growing popularity, making SC more reliable and universal in imaging applications demands overcoming some important technological challenges. We briefly discuss these below. PCF parameters largely determine the underlying spectral broadening and SC stability, so better PCF design and simulation, and their reproducible manufacturing with good fiber quality, is at the heart of tackling many of these challenges.

A. UV Generation

There is great demand to expand the coverage of SC sources to the UV range from 200 to 400 nm and a number of recent efforts have been made in this context [91]. UV coverage would find broad applications in fluorescence microscopy, spectroscopy, and biomedical photonics since many molecules of interest important in cancer and metabolism research, like nicotinamide adenine dinucleotide (NADH) and flavin adenine dinucleotide (FAD), have an intrinsic fluorescence signature when excited by UV light. One scheme to reach UV uses generation of the second, third, and fourth harmonics from a mode-locked Ti:Al_2O_3 laser to go down to 205 nm but it is very complex and features limited tuning capability [92]. If an optical parametric oscillator is used in conjunction, the tunability can be expanded from 250 to 355 nm [93], but the system complexity makes it impractical for general microscopy use. Another technique uses SC generation assisted by cascaded four-wave mixing in a PCF to cover the entire UV-A range (300–400 nm) [22]. An issue with silica-based PCFs is that

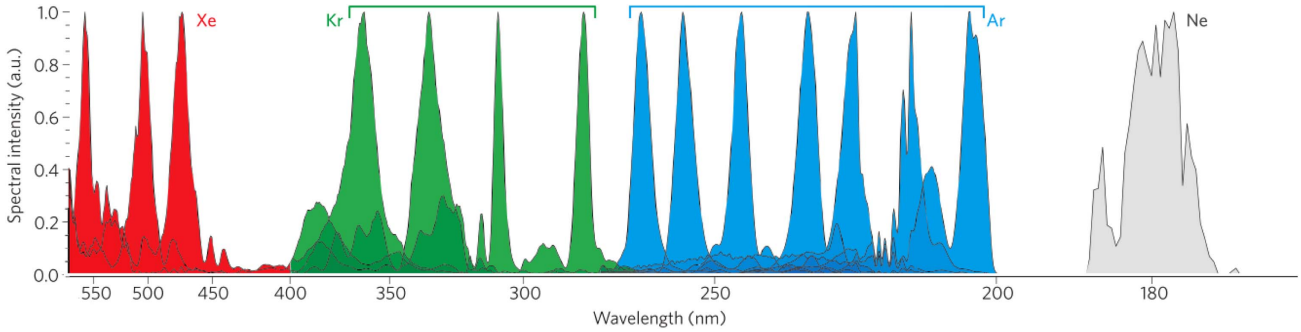

Fig. 9. Coherent ultrashort pulses of tunable bandwidths in the UV range generated in gas-filled hollow-core PCFs, by adjusting pressure and gas mixtures (Ne, Ar, Kr, Xe gases). Adapted from [98] and [12].

they undergo UV damage (solarization) at wavelengths below 380 nm. There have been a few noteworthy advances in the last few years to replace silica in PCFs with exotic glasses like ZBLAN [94] to increase long-term viability. This allows generating a SC with shorter UV wavelengths while still being ultrabroadband, spanning more than three octaves in the 200–2500 nm range. Even relatively low-power and compact laser sources can be used for pumping. Similarly, exciting advances in gas-filled HC fibers, which use photonic bandgaps for trapping and guiding light within a central hollow core [12], have allowed harnessing the UV-transparency and low UV damage susceptibility of gases. While these HC fibers usually suffer from higher propagation losses, certain microstructured designs allow low loss transmission, higher optical damage thresholds, and also exquisite control of fiber nonlinearity and group-velocity dispersion (GVD). A smooth and broadband ADi profile can be achieved simply by varying pressure and gas mixtures [95,96]. The normal GVD of a chosen noble gas can be balanced against the anomalous GVD of a kagome PCF to tune the ZDW across the NIR, visible, and even the UV spectral region. With this level of control, the tunable wavelength can be pushed into the deep-UV and also just as easily into the IR up to 2500 nm, using a relatively low-power and compact laser pump. This has wide-ranging applications in sensing and photochemical studies [97]. The generation of a coherent, ultrafast, deep-ultraviolet signal, optimized to be emitted in a narrow wavelength band tunable from 176 to 550 nm has been demonstrated [12] by varying pressure in inert gases like Ne, Ar, Kr, and Xe (see Fig. 9). The same group also demonstrated the shortest optical wavelength in a SC generated to date, from 124 to 1200 nm using Raman active hydrogen-filled HC PCF [99]. However, all these results from HC PCFs so far have used fs input pulses with microjoule pulse energies (with the exception of a recent paper [100] using 500 nJ pulse energy), which sets the source requirements quite high and current repetition rates in the kilohertz regime make time-resolved imaging very slow. Less stringent source requirements would open the door for widespread use, especially if megahertz repetition rates and high average powers were achievable in the deep-UV to IR range. Simple, compact sources of spatially coherent and ultrafast UV light with long-term stable operation would have excellent application potential in fluorescence microscopy and in the fields of UV absorption spectroscopy, UV-resonant Raman spectroscopy, and laser lithography.

B. Near-Infrared Microscopy

On the other end of the visible spectrum is the near-infrared optical window (650–900 nm), easily accessible using a SC source and silicon-based detectors (for $\lambda < 1000$ nm) with great potential for *in vivo* optical imaging of deep tissues. This 650–900 nm window has minimized light scattering and therefore reduced blur, as well as minimal absorbance by hemoglobin, water, and lipids [101], allowing more photons to reach the detector. Genetically encoded infrared fluorescent proteins would be particularly valuable for whole-body imaging in cancer, stem cell biology, gene therapy, etc. However, the challenges in realizing this opportunity has less to do with SC improvements and more with accessibility and availability of good fluorescent proteins in this range. Over the last few years, the toolbox of fluorescent proteins engineered to push the spectrum further into the IR has been growing [102,103]. Future work targeting improvements in long-term biocompatibility, photostability, and brightness to match the characteristics of widely used fluorophores like green fluorescent proteins (GFPs) will surely open new vistas for *in vivo* deep-tissue imaging in animals. Longer NIR wavelengths have so far been overlooked for imaging due to the lack of appropriate laser sources and suitable detectors. However, with a SC source and the arrival of new IR-CCD photodetectors, such as indium gallium arsenide (InGaAs, λ upto 1700 nm) and indium antimonide (InSb, for $\lambda > 1700$) based detectors, novel imaging opportunities can be realized. Recent research [49] utilizing a SC has identified new optical windows (II: 1100–1350 nm, III: 1600–1870 nm and IV: centered at 2200 nm) with better transmission, minimal absorption, and reduced scattering than the optical window I (650–900 nm) for deep-brain imaging [104].

C. On-Chip Supercontinuum Generation

SC generation has already been demonstrated in various chip-based waveguides. These can become important elements to expand the functionality of photonic integrated circuits or be useful in integrated chip-based imaging applications in the future. SC has been generated in silicon photonic nanowires [105], in silica [106] and chalcogenide [107] waveguides,

although only silicon nitride [108,109] waveguides have allowed pushing the spectrum to broaden toward visible wavelengths for potential on-chip bioimaging applications.

D. Stability with Greater Output Powers

Increasing SC stability while concurrently increasing spectral power density with watt-level total output and broad bandwidth has always been one of the big technological challenges in the SC field. Each of these is easily possible separately (former in fs NDi regime and latter using continuous waves), but combining these two output characteristics using the same pump source has proven to be very difficult, if not impossible, due to the physical mechanisms governing SC generation. Instability in the fs ADi regime has previously been tackled through an alternative approach to solid-core silica PCFs—by using tapered fibers that allow large freedom in controlling the dispersion profile. In the demonstrated tapered fiber [84] tailored to obtain smooth spectra for OCT applications, initial broadening occurs efficiently in the ADi regime. It then evolves into NDi broadening along the taper, resulting in smoother spectra and improved stability due to the NDi. Despite the stability improvement, this approach is not very useful for obtaining greater output powers.

If higher peak powers in a coherent SC from fs pump sources are desired, HC kagome PCFs can again prove to be useful. They can accommodate extremely large pulse energies and higher peak-power fs pulses in the fiber, unlike solid-core PCFs, which would undergo optical damage [99]. Recent advances in gas-filled HC-PCFs with versatile control of dispersion and nonlinearity can allow generating more stable SC [100]. Numerical simulations have shown that the generated dispersive wave pulses in these fibers are highly coherent and independent of input pulse energy when the pulse durations are tens of fs [98]. However, the bigger problem of achieving higher stability with longer pump pulses still exists. Future developments to resolve this issue will enable a huge range of applications.

6. CONCLUSIONS

SC sources provide spectral versatility and spatially coherent, high brightness radiation often at affordable costs and smaller footprint than established tunable laser technologies. The features offered by the compact pulsed SC laser make it an ideal source for fluorescence microscopy and biomedical imaging. Recent advances in novel PCF-based technologies and hollow-core fibers offer promise that current challenges will be surmounted in the near future, offering exciting new opportunites in research laboratories and in the clinic.

Funding. H2020 Marie Skłodowska-Curie Actions (MSCA) (722380); MedImmune; Infinitus (China) Ltd.; Engineering and Physical Sciences Research Council (EPSRC) (EP/H018301/1, EP/L015889/1); Wellcome Trust (089703/Z/09/Z, 3-3249/Z/16/Z); Medical Research Council (MRC) (MR/K015850/1, MR/K02292X/1).

Acknowledgment. C. F. K. acknowledges funding from the EPSRC, Wellcome Trust, MRC, MedImmune, and Infinitus (China), Ltd.

REFERENCES

1. S. W. Hell and J. Wichmann, "Breaking the diffraction resolution limit by stimulated-emission: stimulated-emission-depletion fluorescence microscopy," Opt. Lett. **19**, 780–782 (1994).
2. M. G. L. Gustafsson, "Surpassing the lateral resolution limit by a factor of two using structured illumination microscopy," J. Microsc. **198**, 82–87 (2000).
3. E. Betzig, G. H. Patterson, R. Sougrat, O. W. Lindwasser, S. Olenych, J. S. Bonifacino, M. W. Davidson, J. Lippincott-Schwartz, and H. F. Hess, "Imaging intracellular fluorescent proteins at nanometer resolution," Science **313**, 1642–1645 (2006).
4. M. Rust, M. Bates, and X. Zhuang, "Stochastic optical reconstruction miscroscopy (STORM) provides sub-diffraction-limit image resolution," Nat. Methods **3**, 793–796 (2006).
5. W. Becker, "Fluorescence lifetime imaging—techniques and applications," J. Microsc. **247**, 119–136 (2012).
6. G. Genty, S. Coen, and J. M. Dudley, "Fiber supercontinuum sources (Invited)," J. Opt. Soc. Am. B **24**, 1771–1785 (2007).
7. J. M. Dudley, G. Genty, and S. Coen, "Supercontinuum generation in photonic crystal fiber," Rev. Mod. Phys. **78**, 1135–1184 (2006).
8. P. St. J. Russell, "Photonic crystal fibers," Science **299**, 358–362 (2003).
9. J. Knight, "Photonic crystal fibres," Nature **424**, 847–851 (2003).
10. J. R. Taylor, "Introduction and history," in *Supercontinuum Generation in Optical Fibers*, J. M. Dudley and J. R. Taylor, eds. (Cambridge University, 2010), pp. 1–29.
11. R. R. Alfano, ed., *The Supercontinuum Laser Source* (Springer-Verlag, 2006).
12. P. St. J. Russell, P. Hölzer, W. Chang, A. Abdolvand, and J. C. Travers, "Hollow-core photonic crystal fibres for gas-based nonlinear optics," Nat. Photonics **8**, 278–286 (2014).
13. W. Belardi and J. C. Knight, "Hollow antiresonant fibers with reduced attenuation," Opt. Lett. **39**, 1853–1856 (2014).
14. R. Sollapur, D. Kartashov, M. Zürch, A. Hoffmann, T. Grigorova, G. Sauer, A. Hartung, A. Schwuchow, J. Bierlich, J. Kobelke, M. Chemnitz, M. A. Schmidt, and C. Spielmann, "Resonance-enhanced multi-octave supercontinuum generation in antiresonant hollow-core fibers," Light: Sci. Appl. **6**, e17124 (2017).
15. R. S. Watt, C. F. Kaminski, and J. Hult, "Generation of supercontinuum radiation in conventional single-mode fibre and its application to broadband absorption spectroscopy," Appl. Phys. B **90**, 47–53 (2008).
16. J. Hult, R. S. Watt, and C. F. Kaminski, "High bandwidth absorption spectroscopy with a dispersed supercontinuum source," Opt. Express **15**, 11385–11395 (2007).
17. J. M. Langridge, T. Laurila, R. S. Watt, R. L. Jones, C. F. Kaminski, and J. Hult, "Cavity enhanced absorption spectroscopy of multiple trace gas species using a supercontinuum radiation source," Opt. Express **16**, 10178–10188 (2008).
18. C. F. Kaminski, J. Hult, R. S. Watt, and T. Laurila, "Cavity enhanced spectroscopy of high-temperature H_2O in the near-infrared using a supercontinuum light source," Appl. Spectrosc. **63**, 1389–1395 (2009).
19. T. Udem, R. Holzwarth, and T. W. Hänsch, "Optical frequency metrology," Nature **416**, 233–237 (2002).
20. J. Kasparian, M. Rodriguez, G. Mejean, J. Yu, E. Salmon, H. Wille, R. Bourayou, S. Frey, Y. B. Andre, A. Mysyrowicz, R. Sauerbrey, J. P. Wolf, and L. Woste, "White-light filaments for atmospheric analysis," Science **301**, 61–64 (2003).
21. I. Hartl, X. D. Li, C. Chudoba, R. K. Ghanta, T. H. Ko, J. G. Fujimoto, J. K. Ranka, and R. S. Windeler, "Ultrahigh-resolution optical coherence tomography using continuum generation in an air-silica microstructure optical fiber," Opt. Lett. **26**, 608–610 (2001).
22. A. Labruyère, A. Tonello, V. Couderc, G. Huss, and P. Leproux, "Compact supercontinuum sources and their biomedical applications," Opt. Fiber Technol. **18**, 375–378 (2012).
23. C. F. Kaminski, R. S. Watt, A. D. Elder, J. H. Frank, and J. Hult, "Supercontinuum radiation for applications in chemical sensing and microscopy," Appl. Phys. B **92**, 367–378 (2008).

24. J. K. Ranka, R. S. Windeler, and A. J. Stentz, "Visible continuum generation in air-silica microstructure optical fibers with anomalous dispersion at 800 nm," Opt. Lett. **25**, 25–27 (2000).
25. T. A. Birks, W. J. Wadsworth, and P. St. J. Russell, "Supercontinuum generation in tapered fibers," Opt. Lett. **25**, 1415–1417 (2000).
26. W. Wadsworth, N. Joly, J. Knight, T. Birks, F. Biancalana, and P. St. J. Russell, "Supercontinuum and four-wave mixing with Q-switched pulses in endlessly single-mode photonic crystal fibres," Opt. Express **12**, 299–309 (2004).
27. G. P. Agrawal, *Nonlinear Fiber Optics* (Academic, 2013).
28. A. V. Husakou and J. Herrmann, "Supercontinuum generation of higher-order solitons by fission in photonic crystal fibers," Phys. Rev. Lett. **87**, 203901 (2001).
29. J. Dudley and J. Taylor, *Supercontinuum Generation in Optical Fibers* (Cambridge University, 2010).
30. G. Mcconnell, "Confocal laser scanning fluorescence microscopy with a visible continuum source," Opt. Express **12**, 2844–2850 (2004).
31. C. Dunsby, P. M. P. Lanigan, J. McGinty, D. S. Elson, J. Requejo-Isidro, I. Munro, N. Galletly, F. McCann, B. Treanor, B. Önfelt, D. M. Davis, M. A. A. Neil, and P. M. W. French, "An electronically tunable ultrafast laser source applied to fluorescence imaging and fluorescence lifetime imaging microscopy," J. Phys. D **37**, 3296–3303 (2004).
32. J. A. Palero, V. O. Boer, J. C. Vijverberg, H. C. Gerritsen, and H. J. C. M. Sterenborg, "Short-wavelength two-photon excitation fluorescence microscopy of tryptophan with a photonic crystal fiber based light source," Opt. Express **13**, 5363–5368 (2005).
33. T. Betz, J. Teipel, D. Koch, W. Härtig, J. Guck, J. Käs, and H. Giessen, "Excitation beyond the monochromatic laser limit: simultaneous 3-D confocal and multiphoton microscopy with a tapered fiber as white-light laser source," J. Biomed. Opt. **10**, 054009 (2005).
34. S. Dupont, Z. Qu, S. S. Kiwanuka, L. E. Hooper, J. C. Knight, S. R. Keiding, and C. F. Kaminski, "Ultra-high repetition rate absorption spectroscopy with low noise supercontinuum radiation generated in an all-normal dispersion fibre," Laser Phys. Lett. **11**, 75601 (2014).
35. M. Klimczak, G. Soboń, R. Kasztelanic, K. M. Abramski, and R. Buczyński, "Direct comparison of shot-to-shot noise performance of all normal dispersion and anomalous dispersion supercontinuum pumped with sub-picosecond pulse fiber-based laser," Sci. Rep. **6**, 19284 (2016).
36. J. M. Dudley, G. Genty, and S. Coen, "Fibre supercontinuum generation overview," in *Supercontinuum Generation in Optical Fibers*, J. M. Dudley and J. R. Taylor, eds. (Cambridge University, 2010), pp. 52–61.
37. C. Dunsby and P. M. W. French, "Biophotonics applications of supercontinuum generation," in *Supercontinuum Generation in Optical Fibers*, J. M. Dudley and J. R. Taylor, eds. (Cambridge University, 2010), pp. 349–372.
38. J. R. Clowes, A. B. Grudinin, and I. M. Godfrey, "Flexible and stable supercontinuum source," U.S. patent 9020000 (28April, 2015).
39. K. K. Chen, S.-U. Alam, J. H. V. Price, J. R. Hayes, D. Lin, A. Malinowski, C. Codemard, D. Ghosh, M. Pal, S. K. Bhadra, and D. J. Richardson, "Picosecond fiber MOPA pumped supercontinuum source with 39 W output power," Opt. Express **18**, 5426–5432 (2010).
40. J. C. Travers, A. B. Rulkov, B. A. Cumberland, S. V. Popov, and J. R. Taylor, "Visible supercontinuum generation in photonic crystal fibers with a 400 W continuous wave fiber laser," Opt. Express **16**, 14435–14447 (2008).
41. A. Mussot and A. Kudlinski, "19.5 W CW-pumped supercontinuum source from 0.65 to 1.38 μm," Electron. Lett. **45**, 29–30 (2009).
42. A. Kudlinski and A. Mussot, "Optimization of continuous-wave supercontinuum generation," Opt. Fiber Technol. **18**, 322–326 (2012).
43. A. Periasamy, P. Wodnicki, X. F. Wang, S. Kwon, G. W. Gordon, and B. Herman, "Time-resolved fluorescence lifetime imaging microscopy using a picosecond pulsed tunable dye laser system," Rev. Sci. Instrum. **67**, 3722–3731 (1996).
44. R. Mercatelli, S. Soria, G. Molesini, F. Bianco, G. Righini, and F. Quercioli, "Supercontinuum source tuned by an on-axis monochromator for fluorescence lifetime imaging," Opt. Express **18**, 20505–20511 (2010).
45. P. E. Buchsbaum and J. D. Lane, "Tunable variable bandpass optical filter," U.S. patent 6700690 (March2, 2004).
46. R. Borlinghaus, H. Gugel, P. Albertano, and V. Seyfried, "Closing the spectral gap: the transition from fixed-parameter fluorescence to tunable devices in confocal microscopy," Proc. SPIE **6090**, 60900T (2006).
47. H. Birk, J. Engelhardt, R. Storz, N. Hartmann, J. Bradl, H. Ulrich, L. Microsystems, H. Gmbh, A. Friedensplatz, and D. Mannheim, "Programmable beam-splitter for confocal laser scanning microscopy," Proc. SPIE **4621**, 16–27 (2002).
48. J. H. Frank, A. D. Elder, J. Swartling, A. R. Venkitaraman, A. D. Jeyasekharan, and C. F. Kaminski, "A white light confocal microscope for spectrally resolved multidimensional imaging," J. Microsc. **227**, 203–215 (2007).
49. L. A. Sordillo, L. Lindwasser, Y. Budansky, P. Leproux, and R. R. Alfano, "Near-infrared supercontinuum laser beam source in the second and third near-infrared optical windows used to image more deeply through thick tissue as compared with images from a lamp source," J. Biomed. Opt. **20**, 030501 (2015).
50. B. Redding, M. A. Choma, and H. Cao, "Speckle-free laser imaging using random laser illumination," Nat. Photonics **6**, 355–359 (2012).
51. P. Georgiades, V. J. Allan, M. Dickinson, and T. A. Waigh, "Reduction of coherent artefacts in super-resolution fluorescence localisation microscopy," J. Microsc. **264**, 375–383 (2016).
52. K. Shi, P. Li, S. Yin, and Z. Liu, "Chromatic confocal microscopy using supercontinuum light," Opt. Express **12**, 2096–2101 (2004).
53. C. Olsovsky, R. Shelton, O. Carrasco-Zevallos, B. E. Applegate, and K. C. Maitland, "Chromatic confocal microscopy for multi-depth imaging of epithelial tissue," Biomed. Opt. Express **4**, 732–740 (2013).
54. S. Schlachter, A. Elder, J. H. Frank, A. Grudinin, and C. F. Kaminski, "Spectrally resolved confocal fluorescence microscopy with a supercontinuum laser," Microsc. Anal. **22**, 11–13 (2008).
55. A. Esposito, A. N. Bader, S. C. Schlachter, D. J. van den Heuvel, G. S. K. Schierle, R. V. Ashok, C. F. Kaminski, and H. C. Ger, "Design and application of a confocal microscope for spectrally resolved anisotropy imaging," Opt. Express **19**, 2546–2555 (2011).
56. D. M. Owen, E. Auksorius, H. B. Manning, C. B. Talbot, P. A. A. de Beule, C. Dunsby, M. A. A. Neil, and P. M. W. French, "Excitation-resolved hyperspectral fluorescence lifetime imaging using a UV-extended supercontinuum source," Opt. Lett. **32**, 3408–3410 (2007).
57. T. Zimmermann, J. Rietdorf, and R. Pepperkok, "Spectral imaging and its applications in live cell microscopy," FEBS Lett. **546**, 87–92 (2003).
58. M. Dickinson, G. Bearman, S. Tille, R. Lansford, and S. E. Fraser, "Multi-spectral imaging and linear unmixing add a whole new dimension to laser scanning flourescence microscopy," Biotechniques **31**, 1272–1278 (2001).
59. G. Lu and B. Fei, "Medical hyperspectral imaging: a review," J. Biomed. Opt. **19**, 010901 (2014).
60. V. V. Tuchin, *Tissue Optics: Light Scattering Methods and Instruments for Medical Diagnosis* (SPIE, 2015).
61. K. Suhling, L. M. Hirvonen, J. A. Levitt, P.-H. Chung, C. Tregidgo, A. Le Marois, D. A. Rusakov, K. Zheng, S. Ameer-Beg, S. Poland, S. Coelho, R. Henderson, and N. Krstajic, "Fluorescence lifetime imaging (FLIM): basic concepts and some recent developments," Med. Photon. **27**, 3–40 (2015).
62. H. B. Manning, G. T. Kennedy, D. M. Owen, D. M. Grant, A. I. Magee, M. A. A. Neil, Y. Itoh, C. Dunsby, and P. M. W. French, "A compact, multidimensional spectrofluorometer exploiting supercontinuum generation," J. Biophotonics **1**, 494–505 (2008).
63. D. M. Grant, D. S. Elson, D. Schimpf, C. Dunsby, E. Auksorius, I. Munro, M. A. A. Neil, P. M. W. French, E. Nye, G. Stamp, and P. Courtney, "Optically sectioned fluorescence lifetime imaging using a Nipkow disk microscope and a tunable ultrafast continuum excitation source," Opt. Lett. **30**, 3353–3355 (2005).
64. P. Blandin, S. Lévêque-Fort, S. Lécart, J. C. Cossec, M.-C. Potier, Z. Lenkei, F. Druon, and P. Georges, "Time-gated total internal

reflection fluorescence microscopy with a supercontinuum excitation source," Appl. Opt. **48**, 553–559 (2009).
65. A. D. Elder, C. F. Kaminski, and J. H. Frank, "phi2-FLIM: a technique for alias-free frequency domain fluorescence lifetime imaging," Opt. Express **17**, 23181–23203 (2009).
66. S. Schlachter, A. D. Elder, A. Esposito, G. S. Kaminski, J. H. Frank, L. K. van Geest, and C. F. Kaminski, "mhFLIM: resolution of heterogeneous fluorescence decays in widefield lifetime microscopy," Opt. Express **17**, 1557–1570 (2009).
67. S. Schlachter, S. Schwedler, A. Esposito, G. S. K. Schierle, G. D. Moggridge, and C. F. Kaminski, "A method to unmix multiple fluorophores in microscopy images with minimal a priori information," Opt. Express **17**, 22747–22760 (2009).
68. D. M. Grant, J. Mcginty, E. J. Mcghee, T. D. Bunney, D. M. Owen, C. B. Talbot, W. Zhang, S. Kumar, I. Munro, P. M. P. Lanigan, G. T. Kennedy, C. Dunsby, A. I. Magee, P. Courtney, M. Katan, M. A. A. Neil, and P. M. W. French, "High speed optically sectioned fluorescence lifetime imaging permits study of live cell signaling events," Opt. Express **15**, 15656–15673 (2007).
69. W. Chen, E. Avezov, S. C. Schlachter, F. Gielen, R. F. Laine, H. P. Harding, F. Hollfelder, D. Ron, and C. F. Kaminski, "Method to quantify FRET stoichiometry with phasor plot analysis and acceptor lifetime ingrowth," Biophys. J. **108**, 999–1002 (2015).
70. T. Dertinger and S. Rüttinger, "Advanced FCS: an introduction to fluorescence lifetime correlation spectroscopy and dual-focus FCS," in *Advanced Photon Counting* (Springer, 2014), pp. 89–109.
71. M. Fernandez-Suarez and A. Y. Ting, "Fluorescent probes for super-resolution imaging in living cells," Nat. Rev. Mol. Cell Biol. **9**, 929–943 (2008).
72. D. Wildanger, E. Rittweger, L. Kastrup, and S. W. Hell, "STED microscopy with a supercontinuum laser source," Opt. Express **16**, 9614–9621 (2008).
73. M. D. Lesoine, S. Bose, J. W. Petrich, and E. A. Smith, "Supercontinuum stimulated emission depletion fluorescence lifetime imaging," J. Phys. Chem. B **116**, 7821–7826 (2012).
74. C. Osseforth, J. R. Moffitt, L. Schermelleh, and J. Michaelis, "Simultaneous dual-color 3D STED microscopy," Opt. Express **22**, 7028–7039 (2014).
75. F. Helmchen and W. Denk, "Deep tissue two-photon microscopy," Nat. Methods **2**, 932–940 (2005).
76. E. E. Hoover and J. A. Squier, "Advances in multiphoton microscopy technology," Nat. Photonics **7**, 93–101 (2013).
77. G. McConnell and E. Riis, "Photonic crystal fibre enables short-wavelength two-photon laser scanning fluorescence microscopy with fura-2," Phys. Med. Biol. **49**, 4757–4763 (2004).
78. K. Isobe, W. Watanabe, S. Matsunaga, T. Higashi, K. Fukui, and K. Itoh, "Multi-spectral two-photon excited fluorescence microscopy using supercontinuum light source," Jpn. J. Appl. Phys. **44**, L167 (2005).
79. C. Lefort, R. P. O. Connor, V. Blanquet, L. Magnol, H. Kano, V. Tombelaine, P. Lévêque, V. Couderc, and P. Leproux, "Multicolor multiphoton microscopy based on a nanosecond supercontinuum laser source," J. Biophotonics **9**, 709–714 (2016).
80. J. Yi, W. Liu, S. Chen, V. Backman, N. Sheibani, C. M. Sorenson, A. A. Fawzi, R. A. Linsenmeier, and H. F. Zhang, "Visible light optical coherence tomography measures retinal oxygen metabolic response to systemic oxygenation," Light: Sci. Appl. **4**, e334 (2015).
81. R. A. Costa, M. Skaf, L. A. S. Melo, D. Calucci, J. A. Cardillo, J. C. Castro, D. Huang, and M. Wojtkowski, "Retinal assessment using optical coherence tomography," Prog. Retin. Eye Res. **25**, 325–353 (2006).
82. Z. Zhi, J. Qin, L. An, and R. K. Wang, "Supercontinuum light source enables in vivo optical microangiography of capillary vessels within tissue beds," Opt. Lett. **36**, 3169–3171 (2011).
83. A. Unterhuber, B. Povazay, A. Aguirre, Y. Chen, F. X. Kärtner, J. G. Fujimoto, and W. Drexler, "Broad bandwidth laser and nonlinear optical light sources for OCT," in *Optical Coherence Tomography* (Springer, 2008), pp. 301–358.
84. P. Falk, M. H. Frosz, O. Bang, H. Morioka, S. Takara, O. Kawanishi, K. Kamatani, K. Takiguchi, M. Uchiyama, H. Saruwatari, M. Takahashi, T. Yamada, and H. Kanamori, "Supercontinuum generation in a photonic crystal fiber with two zero-dispersion wavelengths tapered to normal dispersion at all wavelengths," Opt. Express **13**, 7535–7540 (2005).
85. H. Kano and H.-O. Hamaguchi, "Supercontinuum dynamically visualizes a dividing single cell," Anal. Chem. **79**, 8967–8973 (2007).
86. P. Klarskov, A. Isomäki, K. P. Hansen, and P. E. Andersen, "Supercontinuum generation for coherent anti-Stokes Raman scattering microscopy with photonic crystal fibers," Opt. Express **19**, 26672–26683 (2011).
87. T. Gottschall, T. Meyer, M. Baumgartl, C. Jauregui, M. Schmitt, J. Popp, J. Limpert, and A. Tünnermann, "Fiber-based light sources for biomedical applications of coherent anti-Stokes Raman scattering microscopy," Laser Photonics Rev. **9**, 435–451 (2015).
88. H. Kano, H. Segawa, M. Okuno, P. Leproux, and V. Couderc, "Hyperspectral coherent Raman imaging—Principle, theory, instrumentation, and applications to life sciences," J. Raman Spectrosc. **47**, 116–123 (2016).
89. M. Okuno, H. Kano, P. Leproux, V. Couderc, and H. Hamaguchi, "Ultrabroadband multiplex CARS microspectroscopy and imaging using a subnanosecond supercontinuum light source in the deep near infrared," Opt. Lett. **33**, 923–925 (2008).
90. H. Yoneyama, K. Sudo, P. Leproux, V. Couderc, A. Inoko, and H. Kano, "Invited Article: CARS molecular fingerprinting using sub-100-ps microchip laser source with fiber amplifier," APL Photonics **3**, 092408 (2018).
91. J. C. Travers, T. F. Grigorova, and F. Belli, "Ultraviolet supercontinuum generation in optical fibers," in *Conference on Lasers and Electro-Optics* (Optical Society of America, 2018), paper ATu3S.2.
92. A. Nebel and R. Beigang, "External frequency conversion of cw mode-locked Ti:Al_2O_3 laser radiation," Opt. Lett. **16**, 1729–1731 (1991).
93. M. Ghotbi, A. Esteban-Martin, and M. Ebrahim-Zadeh, "Tunable high-repetition-rate femtosecond pulse generation in the ultraviolet," Opt. Lett. **33**, 345–347 (2008).
94. X. Jiang, N. Y. Joly, M. A. Finger, F. Babic, G. K. L. Wong, J. C. Travers, and P. St. J. Russell, "Deep-ultraviolet to mid-infrared supercontinuum generated in solid-core ZBLAN photonic crystal fibre," Nat. Photonics **9**, 133–139 (2015).
95. N. Y. Joly, J. Nold, W. Chang, P. Holzer, A. Nazarkin, G. K. L. Wong, F. Biancalana, and P. St. J. Russell, "Bright spatially coherent wavelength-tunable deep-UV laser source using an Ar-filled photonic crystal fiber," Phys. Rev. Lett. **106**, 1–4 (2011).
96. J. C. Travers, W. Chang, J. Nold, N. Y. Joly, and P. St. J. Russell, "Ultrafast nonlinear optics in gas-filled hollow-core photonic crystal fibers [Invited]," J. Opt. Soc. Am. B **28**, A11–A26 (2011).
97. A. M. Cubillas, S. Unterkofler, T. G. Euser, B. J. M. Etzold, A. C. Jones, P. J. Sadler, P. Wasserscheid, and P. St. J. Russell, "Photonic crystal fibres for chemical sensing and photochemistry," Chem. Soc. Rev. **42**, 8629–8648 (2013).
98. K. F. Mak, J. C. Travers, P. Hölzer, N. Y. Joly, and P. St. J. Russell, "Tunable vacuum-UV to visible ultrafast pulse source based on gas-filled Kagome-PCF," Opt. Express **21**, 10942–10953 (2013).
99. F. Belli, A. Abdolvand, W. Chang, J. C. Travers, and P. St. J. Russell, "Vacuum-ultraviolet to infrared supercontinuum in hydrogen-filled photonic crystal fiber," Optica **2**, 292–300 (2015).
100. P. Hosseini, A. Ermolov, F. Tani, D. Novoa, and P. St. J. Russell, "UV soliton dynamics and Raman-enhanced supercontinuum generation in photonic crystal fiber," ACS Photonics **5**, 2426–2430 (2018).
101. X. Shu, A. Royant, M. Z. Lin, T. A. Aguilera, V. Lev-Ram, P. A. Steinbach, and R. Y. Tsien, "Mammalian expression of infrared fluorescent proteins engineered from a bacterial phytochrome," Science **324**, 804–807 (2009).
102. E. A. Rodriguez, R. E. Campbell, J. Y. Lin, M. Z. Lin, A. Miyawaki, A. E. Palmer, X. Shu, J. Zhang, and R. Y. Tsien, "The growing and glowing toolbox of fluorescent and photoactive proteins," Trends Biochem. Sci. **42**, 111–129 (2017).
103. G. Hong, A. L. Antaris, and H. Dai, "Near-infrared fluorophores for biomedical imaging," Nat. Biomed. Eng. **1**, 0010 (2017).
104. L. Shi, L. A. Sordillo, A. Rodríguez-Contreras, and R. Alfano, "Transmission in near-infrared optical windows for deep brain imaging," J. Biophotonics **9**, 38–43 (2016).
105. I.-W. Hsieh, X. Chen, X. Liu, J. I. Dadap, N. C. Panoiu, C.-Y. Chou, F. Xia, W. M. Green, Y. A. Vlasov, and R. M. Osgood, "Supercontinuum

generation in silicon photonic wires," Opt. Express **15**, 15242–15249 (2007).
106. D. Y. Oh, D. Sell, H. Lee, K. Y. Yang, S. A. Diddams, and K. J. Vahala, "Supercontinuum generation in an on-chip silica waveguide," Opt. Lett. **39**, 1046–1048 (2014).
107. M. R. Lamont, B. Luther-Davies, D.-Y. Choi, S. Madden, and B. J. Eggleton, "Supercontinuum generation in dispersion engineered highly nonlinear (γ = 10/W/m) As_2S_3 chalcogenide planar waveguide," Opt. Express **16**, 14938–14944 (2008).
108. R. Halir, Y. Okawachi, J. S. Levy, M. A. Foster, M. Lipson, and A. L. Gaeta, "Ultrabroadband supercontinuum generation in a CMOS-compatible platform," Opt. Lett. **37**, 1685–1687 (2012).
109. J. P. Epping, T. Hellwig, M. Hoekman, R. Mateman, A. Leinse, R. G. Heideman, A. van Rees, P. J. van der Slot, C. J. Lee, C. Fallnich, and K.-J. Boller, "On-chip visible-to-infrared supercontinuum generation with more than 495 THz spectral bandwidth," Opt. Express **23**, 19596–19604 (2015).